Textures and Microstructures, 1992, Vol. 19, pp. 29–43
Reprints available directly from the publisher.
Photocopying permitted by license only

TEXTURE AND ANISOTROPY BY FORMATION AND DECOMPOSITION OF NICKEL HYDRIDE

I. TOMOV

Institute of Physical Chemistry, Bulgarian Academy of Sciences, 1040 Sofia, Bulgaria

(Received 22 November 1990)

The effect of microstructure and crystal direction on the extent of phase transformation (EPT) of Ni into β-NiH by cathodic charging with H has been investigated by X-ray diffraction, EPT is controlled by the crystal direction in the case of heat-treated specimens. In the case of electrodeposited specimens, the imperfections of which are commensurate with those of cold-worked metals, EPT is controlled by both the crystal direction and the "dislocation-induced" anisotropy at the same time. The decomposition of β-NiH follows the Kolmogorov–Avrami–Johnson–Mehl kinetics. The microstructural anisotropy induces anisotropy in the rate of decomposition of β-NiH.

KEY WORDS Nickel hydride, nickel, electrolytic charging with hydrogen, extent of phase transformation, formation rate anisotropy, decomposition rate anisotropy.

INTRODUCTION

It is well known that as a result of the cathodic charging of nickel with H in the presence of inhibitors, an instable at room temperature nickel hydride phase is produced (Janko 1960, Boniszewski *et al.* 1961, Baranowski 1964, Calbe *et al.* 1964, Borbe *et al.* 1980, Pielaszek 1985). Hydrogen reacts reversibly with nickel by means of the following reaction

$$\mathrm{Ni} + \frac{x}{2}\mathrm{H_2} = \mathrm{NiH}_x$$

where $x = 0.7$–0.8. This is a typical example of a solid-state reaction. The formation of β-NiH is preceded by the formation of α-Ni. α-Ni is a solid solution of about 5 at.% H in Ni and its lattice constant is equal to that of Ni (Pielaszek 1985). Above this mean content, there is an abrupt formation of β-NiH. α-Ni and β-NiH possess a FCC lattice: the lattice constant of β-NiH is 0.3738 nm—it is about 6% greater than the lattice constant of Ni, which is 0.3524 nm (Janko 1960, Pielaszek 1985). β-NiH, formed within the surface layer of the textured electrodeposited Ni, has the same crystallite orientation as the Ni matrix (Majchrzak, Jarmolowicz 1964).

The kinetic analysis of the decomposition of β-NiH was done with the help of volumetric (Baranowski 1959) and X-ray diffraction (Borbe *et al.* 1980, Pielaszek 1985, Janko 1962, Pielaszek 1972, Rashkov *et al.* 1982) methods. Most of these indicated the β-NiH decomposition is expressed, as a rule, by a first-order reaction (Borbe *et al.* 1980, Pielaszek 1985, Baranowski 1959, Janko 1962,

Pielaszek 1972), but there is also a case presented (Rashkov *et al.* 1982) in which the β-NiH decomposition is described by another function. These results (Borbe *et al.* 1980, Pielaszek 1985; Baranowski 1959, Janko 1962, Pielaszek 1972) are irreconcilable with the regularities in the kinetics which have been observed in the formation and decomposition of metal hydrides (Larsen, Livesay 1980, Douglas, Northwood 1983).

In principle, the real structure determines the solid-state transformation rate by its influence both on the chemical decomposition rate (by means of the various defects of the crystal lattice), and on the rate with which the gaseous product reaches or leaves the reaction zone, i.e. the diffusion rate (Delmon 1969). If a property is dependent on the structure, it should then be an anisotropic property, since "the structure anisotropy is a source of anisotropy of the properties" (Bunge 1988). It is known that the diffusion rate is to a great degree dependent on the crystallographic direction (Meyer 1968).

There have been no studies as yet on the effect of the microstructure (crystal size and microdeformations) on β-NiH decomposition. Having in mind these considerations, the purpose of our study was to acquire information on the influence of microstructure anisotropy on the β-NiH formation and decomposition in the various crystal directions. To solve this problem we have employed a suitable X-ray diffraction method. With its help the respective experimental data of previous investigations were processed (Tomov *et al.* to be published).

SPECIMEN PREPARATION AND EXPERIMENTAL

Most of the models for this study were nickel coatings, deposited on $1 \times 25 \times 35$ mm copper substrates. In an X-ray diffraction sense, the 50 μm thick coatings behaved as bulk metal, since their thickness was greater than the effective depth of X-ray penetration (Tomov 1986a). The conditions of electrodeposition were selected in such a way, so as to obtain coatings with differing microstructure and texture. To this end we prepared matt, half-bright, and bright coatings with different surface morphologies. The nickel layers were not detached from their substrates. All specimens given in the tables are representative of 3–4 other specimens.

The cathodic charging of Ni with H was carried out at room temperature in an electrolysis bath consisting of: ln H_2SO_4 and H_2SeO_3–10 mg/l. The duration of cathodic charging was 30 min at a current density of $D_k = 1$ A. dm^{-2}. We charged specimens which were in the as-fabricated state as well as such which were heat treated. The annealed Ni coatings were H-charged after electrolytic polishing. The polishing was carried out in a 60% H_2SO_4 aqueous solution at about 35°C and 40 A. dm^{-2} for 20 s.

EXPERIMENTAL METHODS

The approach to assessing the quantity of β-NiH phase was determined by the specific features of a solid-state reaction. In principle, it starts at the surface and its occurrence is accompanied by the progress of the reaction interface in the

specimen bulk (Delmon 1969). This results in the formation of a hydride layer over the matrix metal. Therefore the problem of assessing the extent of formation or decomposition of nickel hydride is linked to determining the thickness of this layer.

Expressing the Thickness of the Hydride Layer which has Formed

Let us assume that the layer is of a homogeneous composition and that its thickness t is less than the effective depth of X-ray penetration. Then, in the case of a diffractometer, t in any i-direction is expressed by the equation of Friedman and Birks, 1946.

$$t = \frac{\sin\theta}{2\mu_{NiH}} \ln\frac{I}{I_1} \tag{1}$$

where θ is the Bragg angle, μ_{NiH} is the linear absorption coefficient of the hydride, I and I_1 are the integrated intensities of the same diffraction line of Ni before hydrogen charging and at the moment of cessation of H charging (Figure 1a), respectively. Since the i-oriented β-NiH crystallites are formed of i-oriented Ni crystallites (Majchrzak, Jarmolowicz 1964), t accounts only for the phase transformation of crystallites with ideal i-orientation, i.e. t is a measure of the extent of phase transformation (EPT) of Ni into β-NiH in the respective i-crystal direction.

Expressing the Thickness of the Decomposed Hydride

The decomposition process which starts at the specimen surface, results in the formation of a "sandwich" configuration: α-Ni (superficial layer)$\rightarrow$ β-NiH$\rightarrow$ α-Ni (matrix) (Figure 1b). Let us denote the thickness of decomposed hydride layer by t_d. Its lattice contraction brings about the generation of the α-Ni superficial

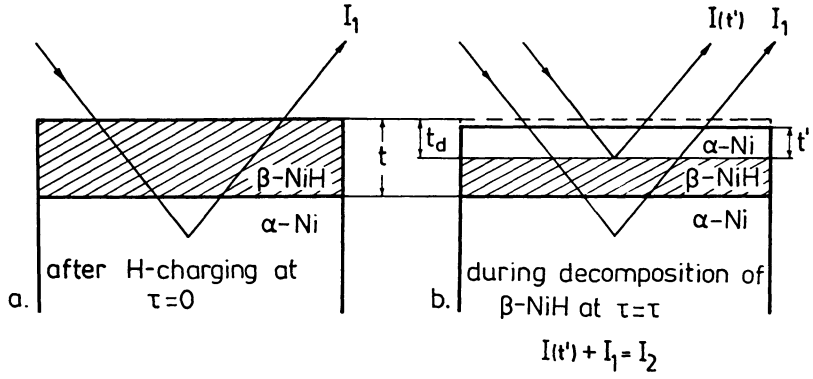

Figure 1 Schematic presentation of the formation (a) and decomposition (b) of a β-NiH layer and the respective change in diffraction conditions; t–β-NiH layer thickness; t_d and t'—thicknesses of the decomposed β-NiH layer and the α-Ni layer which has been generated from it, respectively. Diffracted integrated intensities, immediately after H-charging ($\tau = 0$) I_1, and in any other moment $\tau = \tau$ before complete decomposition I_2.

layer with a thickness of t'. The smaller thickness of t', compared to t_d, is due to the difference in the lattice parameters of α-Ni and β-NiH. The layer with a thickness of t' causes diffraction contributions to the nickel lines, which we denote by $I_{(t')}$. Evidently the total diffracted intensity I_2 is caused by contributions of the α-Ni substrate and α-Ni superficial layer.

$I_{(t')}$ can then be expressed by the difference of I_2 and the I_1 intensity, measured after the cessation of H-charging:

$$I_{(t')} = I_2 - I_1 \tag{2}$$

It is well known (Cullity 1967), that the intensity of a t' thick superficial layer $I_{(t')}$ is linked to the intensity I, diffracted from an infinitely thick specimen through

$$I_{(t')} = I\left[1 - \exp\left(-\frac{2\mu_{\mathrm{Ni}} t'}{\sin\theta}\right)\right] \tag{3}$$

Thus it follows for t'

$$t' = \frac{\sin\theta}{2\mu_{\mathrm{Ni}}} \ln \frac{I}{I - I_{(t')}} \tag{4}$$

After substituting Eq. (2) in Eq. (4), we obtained

$$t' = \frac{\sin\theta}{2\mu_{\mathrm{Ni}}} \ln \frac{I}{I - (I_2 - I_1)} \tag{5}$$

Since absorption is a property of the atom, the superficial layers with thicknesses of t_d and t' absorb X-rays approximately equally, and we may thus write

$$\exp\left(-\frac{2\mu_{\mathrm{Ni}} t'}{\sin\theta}\right) = \exp\left(-\frac{2\mu_{\mathrm{NiH}} t_d}{\sin\theta}\right). \tag{6}$$

In this case we ignore only the X-ray absorption of H evolved as the result of the decomposition process. It follows from Eq. (6) that

$$\mu_{\mathrm{Ni}} t' = \mu_{\mathrm{NiH}} t_d \tag{7}$$

After the substitution of Eq. (7) in Eq. (5), we obtain for the thickness of the decomposed β-NiH layer

$$t_d = \frac{\sin\theta}{2\mu_{\mathrm{NiH}}} \ln \frac{I}{I - (I_2 - I_1)} \tag{8}$$

During the decomposition process I_2 changes within the limits

$$I_1 < I_2 \leq I$$

After the complete decomposition $I_2 = I$ and then Eq. (8) becomes equivalent to Eq. (1). This is a simple way to check the reliability of Eq. (8).

The parameters t and t_d which are linked with the i-direction and thus additionally marked by an i further on—they become t_i and t_{id}. Then the fraction of decomposed hydride F_i is defined as the ratio of the thickness of the decomposed layer t_{id} to the initial thickness t_i, i.e.

$$F_i = \frac{t_{id}}{t_i} \tag{9}$$

There are two reasons which determine the use of the above expressions (Eq. (1) and Eq. (8)) for the correct investigation of the anisotropy of the phase transition:

(1) the orientation distribution of the two phases is analogous, since the "growth" of the β-NiH crystallites during the H-charging is a result of the isotropic increase of the lattice parameter of α-Ni crystallites, as follows from results by Majchrzak and Jarmolowicz 1964, and

(2) the linear absorption coefficient of Ni and NiH are very close.

The effective crystal size D_i and the microdeformations e_i were determined by the single line method (Langford 1978, Delhez *et al.* 1982)

$$\dot{D}_i = \frac{\lambda}{\beta^f_C \cos\theta} \tag{10}$$

$$e_i = \frac{\beta^f_G}{4\tan\theta} \tag{11}$$

where λ is the wavelength, θ is the Bragg angle, β^f_C and β^f_G respectively are the Cauchy (C) and Gaussian (G) components of the integral breadths of the pure diffraction profile (f).

The measurements of the 111, 200, 220 and 311 diffraction lines of α-Ni were performed with an X-ray diffractometer Philips with CuK_α radiation (LiF focusing monochromator). The specimen texture was determined from the poles figures, measured with a texture goniometer. The effective size and the microdeformations of the crystallites in the same directions were determined prior to the cathodic H-charging. To this end we use CoK_β radiation isolated with the help of a LiF focusing monochromator.

The study was carried out at room temperature. The time for measuring the integrated intensity (area) for each line was 100 s, i.e. it is negligible compared to the experimentally established time of decomposition of β-NiH. This leads to the fact that the t_i values are not influenced by effects of the measurement technique.

FORMATION OF β-NiH

EPT of Nickel into Nickel Hydride

If the t values are equal in all i-directions of a given specimen, then we have a case of homogeneous phase transformation. In reality, however, the t_i data given in Table 1 indicate that the phase transformation has occurred to a different degree in the ⟨111⟩, ⟨100⟩, ⟨110⟩, ⟨311⟩ directions in all specimens, i.e. there is an anisotropy of EPT of Ni into β-NiH. Evidently t_i is considerably greater in the ⟨111⟩ and ⟨100⟩ directions than in the ⟨311⟩ and ⟨110⟩ directions.† There are two clearly manifested trends of this nonhomogeneous phase transformation. The

† Because of the presence of a texture it was not possible to measure the 220 lines of α-Ni in all cases, which is the reason for the limited number of t_{110} determinations.

Table 1 Thickness t_i of nickel hydride (β-NiH) in some ⟨hkl⟩ crystal directions of cathodically charged with hydrogen nickel coatings in as-fabricated state. Δt—error due to counting statistics. ⟨uvw⟩—indices of growth texture.

No.	⟨*uvw*⟩	$(t_i \pm \Delta t) \times 10^6$ *m*				*Surface type*
		⟨111⟩	⟨100⟩	⟨110⟩	⟨311⟩	
1	100 + 221	4.1 ± 0.1	3.7 ± 0.1	1.7 ± 0.1	2.5 ± 0.1	matt
2	210 + 542	4.6 ± 0.1	5.8 ± 0.2	1.4 ± 0.1	2.2 ± 0.1	matt
3	211 + 721	4.3 ± 0.1	3.4 ± 0.1		2.2 ± 0.1	matt
4	110 + 411	4.1 ± 0.1	3.5 ± 0.1	1.1 ± 0.1	1.7 ± 0.1	matt
5	100 + 221	5.8 ± 0.2	8.7 ± 0.2		2.1 ± 0.1	half-bright
6	111 + 100	7.6 ± 0.2	9.3 ± 0.2		1.9 ± 0.1	bright

EPT anisotropy of the matt nickel layers (not counting only specimen No. 2 with a ⟨210⟩ texture) can be presented most generally by the inequalities:

$$t_{111} > t_{100} > t_{311} > t_{110} \tag{12}$$

while for the bright, half-bright and matt (with a ⟨210⟩ main texture component) nickel coatings the following inequalities are valid.

$$t_{100} > t_{111} > t_{311} > t_{110} \tag{13}$$

The circumstance that the anisotropy of the phase transformation is described by two inequalities ((12) and (13)) gives us grounds to assert that EPT depends both on the crystal direction and the microstructure anisotropy. The main problem is how to distinguish the influence of the different structure parameters on EPT. This requires the next step of our study to be linked to obtaining information on the effective crystal size and microdeformations.

Effect of Microstructure Anisotropy on EPT

The microstructure parameters were determined prior to the specimen charging with H. Table 2 lists the values of the effective crystal size D_i (upper lines) and microdeformations e_i (lower lines). D_i of all matt coatings (specimens Nos. 1–4) in all crystal directions are considerably greater than the D_i of the bright coatings (specimen No. 6). Moreover, these results indicate that D_i is anisotropic. A specific characteristic of the grain size anisotropy is that D_i is largest in the direction of the main texture component (Surnev, Tomov 1989). This is confirmed in this case too: the effective crystal size is greatest in the ⟨100⟩, ⟨110⟩, ⟨100⟩ and ⟨111⟩ directions for specimens Nos. 1, 4, 5, 6, respectively.†

The results indicate the specificity of the grain size anisotropy for each concrete growth texture, and that it does not correlate with the anisotropy of

† It was impossible to measure the effective crystal size D_i in the ⟨210⟩ and ⟨211⟩ directions with CoK_β-radiation because of technical considerations.

Table 2 Effective size D_i (upper lines) and microdeformations e_i (lower lines) of the crystallites in some ⟨hkl⟩ directions before cathodically charging with hydrogen of the Ni electrodeposited layers. X-ray diffraction measurements with CoK_β-radiation. LiF focusing monochromator.

No.	$D_i \pm \Delta D$ [*nm*]—*upper line* $(e_i \pm \Delta e) \cdot 10^3$—*lower line*			
	⟨111⟩	⟨100⟩	⟨110⟩	⟨311⟩
1	91 ± 7	*>150*		*59 ± 6*
	1.5 ± 0.2	1.5 ± 0.1		1.3 ± 0.1
2	87 ± 6	56 ± 4		23 ± 2
	2.8 ± 0.2	4.1 ± 0.2		1.5 ± 0.2
3	45 ± 3	38 ± 4		52 ± 6
	1.5 ± 0.2	3.5 ± 0.4		2.2 ± 0.2
4	49 ± 6	44 ± 7	96 ± 8	40 ± 5
	1.5 ± 0.2	1.5 ± 0.2	2 ± 0.2	1.7 ± 0.2
5	32 ± 4	94 ± 8		22 ± 5
	3.6 ± 0.3	5.1 ± 0.4		3.3 ± 0.3
6	28 ± 4	17 ± 2		19 ± 3
	4.1 ± 0.2	7.9 ± 0.6		5.4 ± 0.4

phase transformation as expressed by the two series of inequalities (12) and (13). But it is also evident that EPT falls continuously with the increase in D_i, i.e. from bright to matt coatings (compare Table 1 with Table 2).

The papers (Prelaszek 1985, 1972) discuss the role of dislocations in β-NiH formation. We shall on the basis of our experimental results attempt to assess the role of microdeformations on the EPT. By origin they are linked mainly with the tension fields around dislocations in the crystal interior (Bever *et al.* 1973), which is the reason the microdeformations to be used as a measure for assessing the dislocation density (Williamson and Smollman 1956). The dislocation density in electrodeposited metals (Hinton *et al.* 1963; Hofer *et al.* 1965) is commensurate with that of cold-worked metals (Read, Shokley 1952), for which it is 10^{11} to 10^{12} dislocations per cm^2. The values which we have obtained for the dislocation density from D_i and e_i data (see Table 2), according to Williamson and Smollman 1956, are within the limits 8×10^{10} to 2×10^{12} dislocations per cm^2. We established the highest dislocation density for bright coatings (specimen No. 6), and the lowest—for matt coatings (specimen No. 1). Because of the existing analytical connection between the microdeformations and dislocation density, the two terms will be used interchangeably.

The microdeformation values increase in the order from matt to bright coatings. Within the set of matt coatings this order depends in addition on the texture. The e_i distribution has an anisotropic character. Thus for most of the specimens the results reveal a trend for relatively higher microdeformations in the ⟨100⟩ direction compared to the other crystal directions. This trend is especially clearly expressed for specimens Nos. 2, 5, 6 (Table 2) for which e_i are very high. In fact, inequalities (13) are valid for specimens Nos. 2, 5, 6. These facts undoubtedly confirm that the dislocation-induced anisotropy causes anisotropy of EPT and that the dislocations strongly favour the phase transformation of Ni into

β-NiH. They are in agreement with the assumption made by Atreus *et al.* 1980, Latanision 1983 that the dislocations act as H traps and in thus support the model for the role of dislocations for the formation of β-NiH (Pielaszek 1985, 1972).

The question arises what changes would occur with anisotropy of phase transformation, if the dislocation-induced anisotropy is eliminated. This determined the next step in our study to be to investigate the influence of the crystal structure obtained as a result of annealing processes (recovery, recrystallization, grain growth) on the EPT of Ni into β-NiH.

EPT of Ni into β-NiH in Thermally Treated Specimens

The thermal treatment of the above specimens was carried out at 520°C in an argon atmosphere (purified of O_2) for five hours. The data on the recrystallization texture obtained from the analysis of the pole figures are presented in Table 3, column $\langle uvw \rangle$. In fact, the specimens now possess a new structure, and this is reflected in their notation by the addition of a '-mark. In all cases was observed the $\langle 100 \rangle$ recrystallization component, but for specimens Nos. 2, 4 were also observed the $\langle 110 \rangle$ and $\langle 210 \rangle$ main components of recrystallization texture, respectively. As a result of the recrystallization some crystallites had grown considerably, the consequence of which was that they had their own detectable reflections on the pole figures. According to Hirsch 1956, it may be considered as established that the annealed metals contain 10^6 to 10^8 dislocations per cm^2, which means that the dislocation density of our specimens is 3–4 orders of magnitude lower than that of their nonannealed state. This determines a reduced permeation of H in Ni crystallites as has been discussed for an analogous case by Paatsch 1988. As a rule the annealing process leads to the onset of a similarity in the texture, crystal size, and dislocation density. This similarity reflects on a common for all specimens decrease in t_i compared to its values for the nonannealed state. Thus stands out the sharp decrease in t_{100} for specimens Nos. 2, 5, 6 which in some cases is 2–4 times less than t_{100} for the nonannealed state of the same specimens. By means of the experiments with annealed specimens for which the transport of H toward the interior is hindered, because of the lowered dislocation density and diminished grain boundaries area (because of the increased crystallite size), the promoting role of these two structure parameters on EPT is again revealed.

Table 3 Thickness t_i of nickel hydride (β-NiH) in some $\langle$hkl$\rangle$ crystal directions of cathodically charged with hydrogen nickel coatings after heat treatment. Δt—error due to counting statistics. $\langle$uvw$\rangle$—indices of recrystallization texture.

No.	$\langle uvw \rangle$	$(t_i \pm \Delta t) \times 10^6\, m$			
		$\langle 111 \rangle$	$\langle 100 \rangle$	$\langle 110 \rangle$	$\langle 311 \rangle$
1′	100 + 221	3.2 ± 0.1	1.9 ± 0.1	1.1 ± 0.1	1.7 ± 0.1
2′	100 + 110 + 210	2.9 ± 0.1	2.1 ± 0.1	1.4 ± 0.1	1.8 ± 0.1
3′	100 + 221	3.3 ± 0.1	1.9 ± 0.1		1.5 ± 0.1
4′	100 + 210 + 110	3.1 ± 0.1	2.1 ± 0.1	0.9 ± 0.1	1.6 ± 0.1
5′	100 + 221	3.0 ± 0.1	2.0 ± 0.1		1.8 ± 0.1
6′	100 + 111	3.1 ± 0.1	2.2 ± 0.1	1.2 ± 0.1	1.6 ± 0.1

The EPT anisotropy in the investigated crystal directions is described by the inequalities (12) for all thermally treated specimens. Therefore after annealing, that is after eliminating the influence of the dislocation-induced anisotropy, it becomes evident that the main factor which affects EPT is the crystallographic direction. This is one of the most important results of our study.

DECOMPOSITION KINETICS OF β-NiH AT ROOM TEMPERATURE

It is well known that the kinetic behaviour exhibited by hydriding and dehydriding processes (Larsen *et al.* 1980, Douglas *et al.* 1983, Rudman 1979) is similar to that of many of the phase transformations of the nucleation and growth type, i.e. the summary transformation process is described by the equation of Kolmogorov (1937), Avrami (1939), Johnson and Mehl (1939)

$$F_i(\tau) = 1 - \exp\left[-\left(\frac{\tau}{\tau_i}\right)^k \right] \tag{14}$$

where $F_i(\tau)$ is the β-NiH volume fraction corresponding to the i-direction, k is a number, the value of which is dependent on the geometry linked with the rate-controlling process, τ_i is the reaction rate time constant. The last has a clear physical sense—this is the time $\tau = \tau_i$, for which the decomposed volume fraction $F_i(\tau_i)$ has a constant value.

$$F_i(\tau_i) = \frac{e-1}{e} \cong 0.6322, \tag{15}$$

as follows from (14). The values of the parameters τ_i and k were determined by computer fitting of the $F_i(\tau)$ relations (14) to the experimental data. The values of the k exponent are within the interval 1.5–4, the lower values pertaining to recrystallized large crystalline specimens and the greater values referring to unannealed fine crystalline such.

An illustration for the decomposition kinetics of an unannealed half-bright coating is given by Figure 2. Since the decomposition process proceeds in the two investigated by us $\langle 111 \rangle$ and $\langle 100 \rangle$ directions at the same rate, Figure 2 shows the kinetic curve only for the $\langle 100 \rangle$ direction. An example for a decomposition in the same directions of NiH formed in the recrystallized specimen No. 3′ (obtained after heat treatment of specimen No. 3) is presented in Figure 3. The results we have presented unambiguously show that the decomposition process both for annealed and unannealed specimens are controlled by the Avrami, Johnson-Mehl kinetics. Our results do not confirm the occurrence of a reaction of the first order. It is evident, however, that the decomposition process in the annealed specimen proceeds at a different rate in the $\langle 111 \rangle$ and $\langle 100 \rangle$ directions. The last fact has been linked to the microstructure anisotropy in the specimen, which has appeared as a result of its H-charging.

A qualitative assessment of the microstructure in the $\langle 111 \rangle$ and $\langle 100 \rangle$ directions of specimen No. 3′ can be made from the profile of the 111 and 200 diffraction lines, measured after the decomposition of β-NiH (Figure 4). The value of the microdeformations in crystallites with an $\langle 111 \rangle$ orientation is about 1.5×10^{-3}, while the microdeformations in the $\langle 100 \rangle$-direction are below the

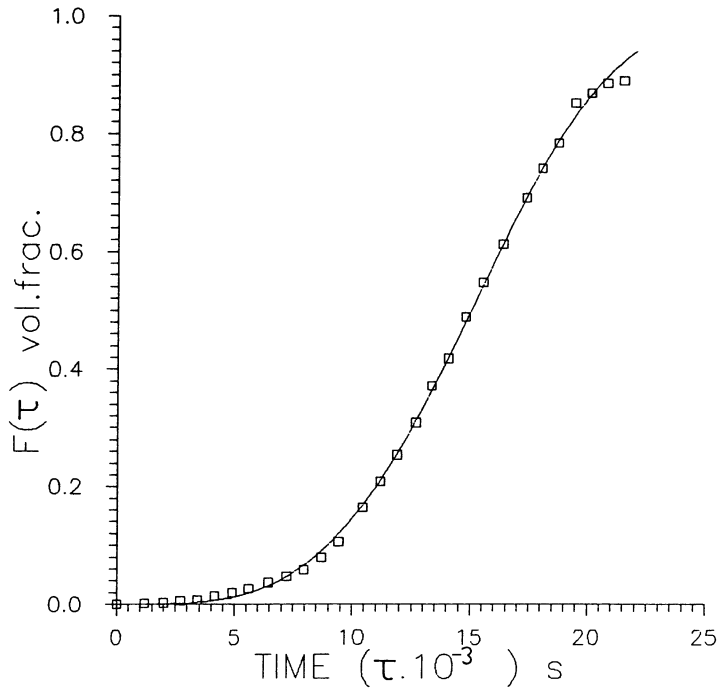

Figure 2 Decomposition kinetics of β-NiH, formed in electro-deposited half-bright nickel (specimen No. 5). $F(\tau)$—volume fraction of nickel hydride which has decomposed in the ⟨100⟩ direction.

sensitivity of this measurement method. Pielaszek has also established that there are no isotropic deformations generated during the hydride formation-decomposition cycle (neither are there any deformations in the ⟨100⟩ direction). This information reveals in a qualitative aspect the effect of the microstructure anisotropy on the anisotropy of the decomposition rate. This phenomenon can, however, be assessed quantitatively for all specimens.

Anisotropy of the β-NiH Decomposition Rate

The β-NiH decomposition rate can be derived by differentiating Eq. (14)

$$\frac{dF_i(\tau)}{d\tau} = Q_i(\tau) = k\left(\frac{1}{\tau_i}\right)^k \tau^{k-1} \exp\left[-\left(\frac{\tau}{\tau_i}\right)^k\right] \tag{16}$$

For the studied directions of all specimens this rate can be assessed by means of its value Q_{max} at the point of inflection. Q_{max} is the NiH volume fraction, undergone transformation per unit time, at the moment the maximal process rate is achieved. These values are presented in Table 4. The different Q_{max} in the various i-crystal directions for a given specimen are evidence that there is an anisotropy in the decomposition rate, which can depend on both crystal direction and Ni microstructure.

To evaluate the effect of microstructure alone on the dehydriding rate $Q_i(\tau)$, Figure 5 compares kinetic data on the ⟨100⟩ crystal direction for specimens with

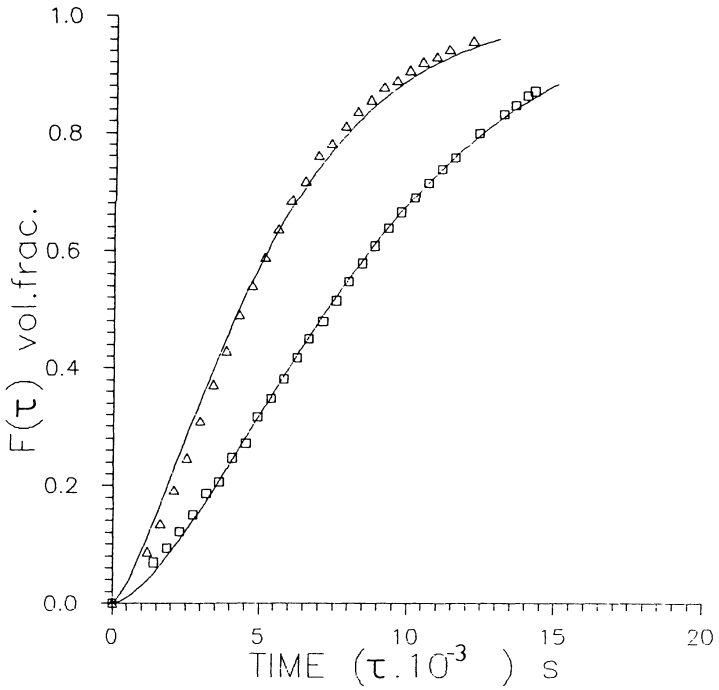

Figure 3 Anisotropy in the kinetics of decomposition of β-NiH, recrystallized after thermally treating Ni (specimen No. 3'). $F(\tau)$—volume fraction of the hydride which has decomposed in the ⟨111⟩-Δ and ⟨100⟩-□ directions.

considerably differing microstructures (Nos. 1, 5, 6—see Table 2). The differential kinetic curves $Q_i(\tau)$ were calculated according to Eq. (16), in which the parameters τ_i and k were determined by fitting Eq. (14) to the respective experimental data. The life-time of the hydride phase is greatest for specimen No. 6, which has the highest microdeformations and the smallest crystallites (the greatest area of grain boundaries). It is known that the defects and grain boundaries are sites which can act as H traps (Atrens *et al.* 1980, Latanision *et al.* 1983). On the basis of diffusion studies, a list is given by Atrens *et al.* 1980 of the approximate values of the interaction energies between the trap and H atom for different trap types (point, line and planar trapping defects). The binding energy of trapping is lowest for point defects, and highest for dislocations, i.e. the last are the traps with the greatest depth. From such a point of view, the different differential curves in Figure 5 can be explained by the varying density and efficiency of the traps. This effect reflects the expected microstructure influence (form and size of the crystallites and density of their defects) on the chemical reaction rate (Delmon 1969), which in fact, means on the hydride phase stability.

The intrinsic parameter for characterizing the NiH stability is the reaction time constant τ_i. It has been defined from the condition which follows from Eq. (15). The τ_i values characterize the hydride stability at room temperature (Table 4). In the case of unannealed large crystalline specimens Nos. 1 and 3, the τ_i values are

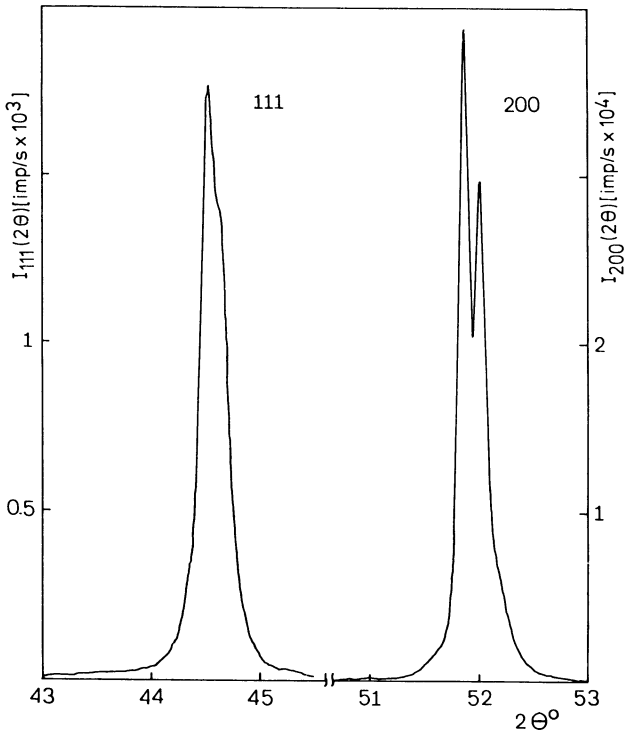

Figure 4 Profile of the diffraction lines 111 and 200 of specimen No. 3′, after the decomposition of β-NiH.

Table 4 Maximal decomposition rate Q_{max} (volume fraction per second) and decomposition rate time constant τ_i of β-NiH in the ⟨111⟩ and ⟨100⟩ directions of specimens with different textures.

No.	$Q_{max} \times 10^5$ [vol. frac. $\times s^{-1}$]		τ_i [s]	
	⟨111⟩	⟨100⟩	⟨111⟩	⟨100⟩
1	18.2	17.1	8,860	7,370
3	12.0	10.6	5,990	5,800
3′	15.6	8.1	5,600	9,220
5	10.3	10.2	16,510	16,600
6	4.6	4.5	25,015	25,200

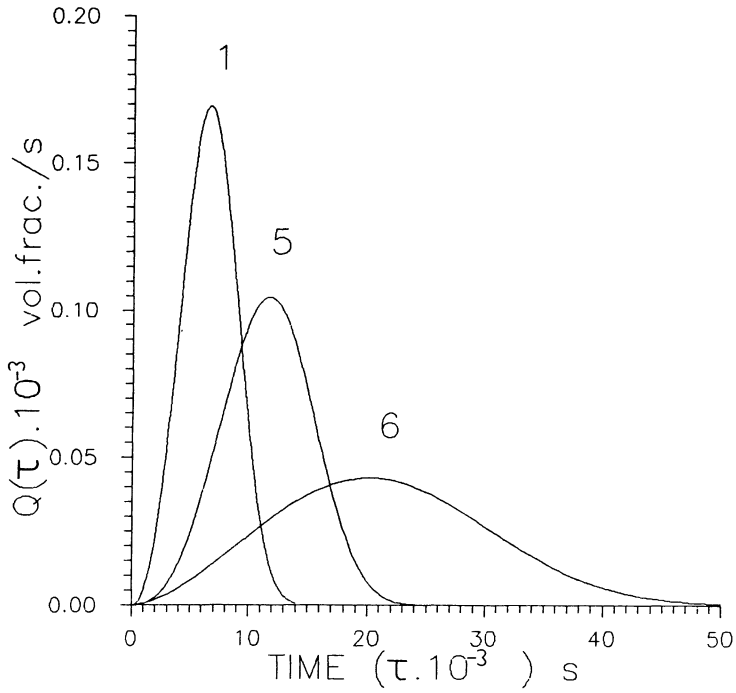

Figure 5 Differential kinetic curves presenting the decomposition rate $Q_i(\tau)$ of β-NiH in the $\langle 100 \rangle$ direction of specimens Nos. 1, 5, 6.

considerably lower than for fine crystalline coatings with great microdeformations, i.e. for the specimens Nos. 5 and 6.

CONCLUSION

The phase transformation of Ni into β-NiH is anisotropic. Our studies indicate that the anisotropy of EPT in polycrystals, consisting of crystallites with lattice imperfections, is controlled by two factors:

(1) crystallographic direction, i.e. orientation of the crystallites versus surface of charging with H.

(2) "dislocation induced" anisotropy, i.e. the orientation distribution of dislocation density.

In the case of polycrystals, consisting of "perfect" crystallites which have grown during the annealing process, the anisotropy of the phase transformation is controlled by one main factor—the crystallographic direction.

The discussion so far indicates that the mean EPT value should depend not only on dislocation density, but also on the texture (through the distribution of the occurring crystal directions) and on the mean crystallite size (through the area of the grain boundaries).

The different EPT observed in the different crystal directions is in essence an indication for the occurrence of an orientation dependent process during the

charging of Ni with H. The orientation dependence of EPT of Ni into β-NiH undoubtedly is a consequence of the differing rates of permeability of H in the relevant crystal directions of a Ni polycrystal.

The kinetic analysis of the β-NiH dehydriding indicates that the transformation rate is dependent on the structure of the medium where the chemical reaction proceeds. We have to emphasize that the grain boundaries and dislocations may have a two-fold action on the phase transition: as *a shortened diffusion paths in the H transport,* and as *H traps by chemical reaction.*

The cases of β-NiH decomposition which we have discussed do not concern kinetics of a first order reaction, such as has been reported in. Such an order of kinetics have some of the homogeneous reactions whose elementary chemical act is carried out with the same probability in all sites of the reaction system. The reaction rate is then proportional to the concentration of one of the reacting components. This is not the case, however, of a solid-state reaction, which was the subject of our study.

ACKNOWLEDGEMENTS

The authors would like to thank M.Sc. S. Surnev, Department of Solid State Physics, Sofia University for the computer fitting of the relevant experimental data.

References

Atrens, A., Mezzanote, D., Fiore, N. F. and Genshaw, A. (1980). *Corros. Sci.,* **20,** 673.
Avrami, M., *J. Chem. Phys.,* (1939) **7,** 1103; (1940) **8,** 212; (1941) **9,** 177.
Baranowski, B. (1959). *Bull. Acad. Polon. Sci. (ser. sci. chim.),* **7,** 891.
Baranowski, B. (1964). *Roczniki Chemii Ann. Soc. Chim. Polon.,* **38,** 1019.
Bever, M. B., Holt, D. L. and Titchner, A. l. (1973). In *Progress in materials science,* eds. B. Chalmers, J. W. Christian and T. B. Massalski, v. **17,** Pergamon Press, Oxford.
Boniszewski, T. and Smith, G. C. (1961). *J. Phys. Chem. Solids,* **21,** 115.
Borbe, P. Ch., Erdmann-Jesnitzer, F. and Schoebel, W. (1980). *Z. Mettallkunde,* **71,** 227.
Bunge, H. J. In *Directional properties of materials,* ed. H. J. Bunge, DGM Informationsgeselschaft-Verlag, 1.
Calbe, I. W., Wollan, E. O. and Kocher, W. H. (1964). *Le J. de Phys.,* **25,** 460.
Cullity, B. D. (1967). *Elements of X-Ray diffraction,* Addison and Wesley Publ. Co., London, 269.
Delhez, R., Kaijser, Th. H. de and Mittemeijer, E. J. (1982). *Fres. Z. Anal. Chem.,* **112,** 1.
Delmon, B. (1969). *Introduction a la cinetique heterogene,* Editions Technip., Paris, (russian transl.) 379, 413.
Douglas, I. G. and Northwood, D. O. (1983). *J. Mater. Sci.,* **18,** 321.
Friedmann, H. and Birks, L. S. (1946). *Rev. Sci. Instrum.,* **17,** 99.
Hinton, R. W., Schwartz, L. H. and Cohen, J. B. (1963). *J. Electrochem. Soc.,* **110,** 103.
Hirsch, P. B. (1956). *Progr. Metal Phys.,* **6,** 236.
Hofer, E. M. and Hintermann, H. E. (1965). *J. Electrochem. Soc.,* **112,** 167.
Janko, A. (1960). *Bull. Acad. Polon. Sci. (ser. sci. chim.),* **8,** 131; (1960) *Naturwiss.* **47,** 225.
Janko, A. (1962). *Bull. Acad. Polon. Sci. (ser. sci. chim).,* **10,** 617.
Johnson, W. A. and Mehl, R. F. (1939). *Trans. Amer. Inst. Min. (Metall) Engrs,* **135,** 416.
Kolmogorov, A. (1937). *Bull. Acad. Sci. USSR (sci. math. natur.),* **3,** 355.
Langford, J. I. (1978). *J. Appl. Cryst.,* **11,** 10.
Larsen, J. W. and Livesay, B. R. (1980). *J. Less-Common Metals,* **73,** 79.
Latanision, R. M. and Kurkela, M. (1983). *Corrosion-Nice,* **39,** 174.
Majchrzak, S. and Jarmolowicz, H. (1964). *Bull. Acad. Polon. Sci. (ser. sci. chim.),* **12,** 155.

Meyer, K. (1968). *Physikalisch-Chemische Krystallographie,* VEB Deutscher Verlag fuer Grundstoffindustrie, Leipzig (russian transl. p. 243).
Paatsch, W. (1988). *Plat. and Surf. Fin.*, **75,** 52.
Pielaszek, (1972). *J. Bull. Acad. Polon. Sci.* (*ser. sci. chim*), **20,** 484.
Pielaszek, J. (1972). *Bull. Acad. Polon. Sci.* (*ser. sci. chim.*), **20,** 611.
Pielaszek, J. (1985). In *Hydrogen degradation of ferrous alloys,* eds. R. A. Oriani, J. P. Hirth and M. Smialowski, New Public. Park Ridge, USA, 167.
Rashkov, St., Monev, M. and Tomov, I. (1982). *Surf. Technology,* **16,** 203.
Read, W. T. and Schockley, W. (1952). *Imperfections in nearly perfect crystals,* Wiley, New York, 166.
Rudman, R. S. (1979). *J. Appl. Phys.*, **50,** 7195.
Surnev, Sv. and Tomov, I. (1989). *J. Appl. Electrochem.*, **19,** 75.
Tomov, I. *phys. stat. sol.* (*a*), (1986) **95,** 397; (1986) **98,** 43.
Tomov, I. and Monev, M., to be published.
Tomov, I., Monev, M., Mikhailov, M. and Rashkov, St., to be published.
Wiliamson, G. K. and Smollman, R. E. (1956). *Phil. Mag.*, **1,** 34.